Biophysical Chemistry 157 (2011) 1–6

Contents lists available at ScienceDirect

Biophysical Chemistry

journal homepage: http://www.elsevier.com/locate/biophyschem

Structural basis for the role of LYS220 as proton donor for nucleotidyl transfer in HIV-1 reverse transcriptase

Servaas Michielssens [a,*], Samuel L.C. Moors [a], Mathy Froeyen [b], Piet Herdewijn [b], Arnout Ceulemans [a]

[a] Departement of Chemistry and INPAC Institute of Nanoscale Physics and Chemistry, Katholieke Universiteit Leuven, Leuven, Belgium
[b] Rega Institute for Medicinal Research, Katholieke Universiteit Leuven, Leuven, Belgium

ARTICLE INFO

Article history:
Received 22 February 2011
Received in revised form 25 March 2011
Accepted 26 March 2011
Available online 5 April 2011

Keywords:
HIV reverse transcriptase
QM/MM
Molecular dynamics
Protein dynamics
Enzymatic catalysis

ABSTRACT

Biochemical studies by Castro et al. have recently revealed a crucial role for a general acid in the catalysis of nucleic acid transfer in distinct classes of polymerases. For HIV-RT LYS220 was identified as proton donor. This was unanticipated from a structural point of view, since in all ternary crystal structures of HIV-RT LYS220 are too distant from the active site to fulfill this role. In this work molecular dynamics simulations were used to reveal the dynamics of HIV-RT and to provide structural evidence for the role of LYS220. During a 1 μs molecular dynamics simulation LYS220 migrates toward the active site and occupies several positions enabling direct and water mediated proton transfer towards pyrophosphate. A combination of quantum mechanical and molecular mechanics methods was used to validate the different modes of interaction.

1. Introduction

HIV reverse transcriptase is a critical enzyme in the HIV life cycle, catalyzing the transcription of the viral RNA to DNA. It is also a target for numerous drugs. Detailed knowledge of the catalytic mechanism is vital to rationally develop nucleoside like drugs that cause chain termination [1]. The active site and reaction are schematically represented in Fig. 1. Nucleophilic attack on the phosphorus atom of the ribonucleoside triphosphate by the primer 3′-hydroxyl leads to the formation of a phosphodiester bond and release of pyrophosphate. Two Mg^{2+} ions are present in the active site. Mg^{2+} A lowers the pKa of the primer's 3′-hydroxyl to facilitate the initial proton transfer [2,3]. Mg^{2+} B has a structural role, it stabilizes the negative charge in the transition state and might help the release of pyrophosphate [4,5]. A second proton transfer involves the protonation of triphosphate [6].

The acceptor for the first proton transfer is still unknown. Potential acceptors are ASP186 or water. The donor of the second proton transfer was recently identified by Castro et al. by sequence alignment and confirmed by biochemical studies [7]. It was found that LYS220 fulfills this role in HIV-RT. Moreover, lysine was revealed to function in several classes of polymerases as general acid. However, structural evidence for the role of LYS220 is missing since it is not situated near the active site in any of the ternary crystal structures of HIV-RT[8–10]. In Fig. 2 the position of LYS220 in the crystal structure is shown (the position of LYS220 in the crystal structure is indicated by the blue color, the code of the crystal structure used is 1RTD). The side chain nitrogen of LYS220 is located more than 1.5 nm from the active site. This crystal structure cannot give a structural justification for its role in the catalysis. Molecular dynamics simulations in this work reveal the dynamics of this residue and provide the necessary structural evidence.

2. Methods

2.1. Molecular dynamics

2.1.1. Model building

The simulation was started from the 1RTD crystal structure [10]. The p66 unit, including DNA was used for the simulations. The base of the entering tymidine triphosphate was modified to an adenine and the complementary adenine base (E5) was changed into a thymine by an inverse fitting procedure using Quatfit (Quatfit program in CCL software archives).

The AMBER 99SB force field was used for the DNA and the protein [11]. It was verified that the DNA backbone parameters α and γ stayed close to their canonical value, since transition to unrealistic values is a known problem for free DNA simulations in the AMBER force field [12]. The triphosphate parameters were taken from Meagher et al. [13]. Protonation states were calculated using the H++−server [14] and confirmed by the PROPKA server [15]. The 3′-hydroxyl group of the primer strand is missing in the crystal structure and was added

* Corresponding author at: Celestijnenlaan 200F, 3001 Heverlee, Belgium. Tel.: +32 16 327384; fax: +32 16 327992.
E-mail address: servaas.michielssens@chem.kuleuven.be (S. Michielssens).

0301-4622/$ – see front matter © 2011 Elsevier B.V. All rights reserved.
doi:10.1016/j.bpc.2011.03.009

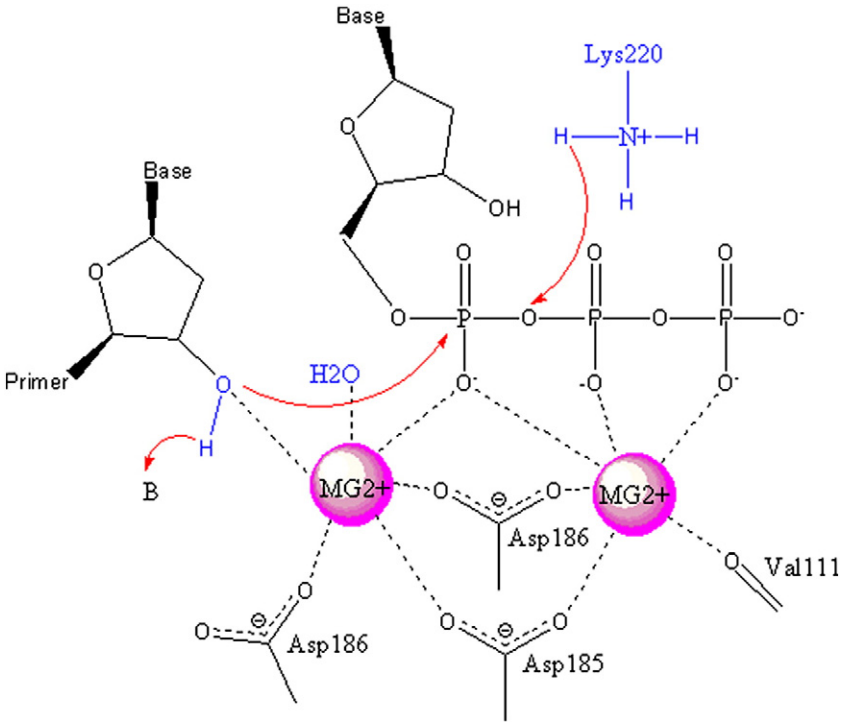

Fig. 1. Schematic representation of the reaction and active site of HIV-RT. Nucleophilic attack on the-phosphorus atom of the ribonucleoside triphosphate by the primer 3′-hydroxyl leads to the formation of a phosphodiester bond and release of pyrophosphate. Catalytic Mg^{2+} cations and their coordination shell are represented. Parts not present in the active site of the crystal structure but which occur after modeling (3′-hydroxyl) and MD-simulations (water and lys220) are colored blue.

using tleap [16]. The AMBER topology and structure file were converted to GROMACS using amb2gmx [17,18].

2.1.2. Simulation setup

A dodecahedral simulation box was added. The dimensions were set to the diameter of the system (largest distance between 2 atoms) plus twice 0.8 nm. The system was solvated with 38349 TIP3P water molecules [19]. To neutralize the system 32 sodium ions were added. The total system consists of 125 661 atoms. The GROMACS simulation package [20] was used to simulate the neutralized solvated system. Long-range electrostatics were computed with the particle mesh Ewald method [21]. The non-bonded cutoff was set to 1.1 nm. A Fourier spacing of 0.12 nm was used. All covalent bonds were constrained using P-LINCS [22]. A timestep of 2 fs was used.

The system was first minimized using the steepest descent method, followed by a slow heating of the system from 0 to 300 K during 500 ps. Next the system was subjected to 500 ps of equilibration at 300 K, to equilibrate the energy. The system temperature was controlled by the velocity rescaling thermostat [23] and the pressure was controlled using the Parinello-Rhaman barostat [24]. Finally the system was simulated in a production run of 1 μs.

2.2. QM/MM optimizations

2.2.1. Methods

The QM/MM calculations were done with a two-layer ONIOM [25–27] approach. The selected model system (Fig. 3) was treated with density functional theory (DFT) with the B3LYP [28] functional and DGDZVP basis set [29,30], the rest of the system was treated with the AMBER 99SB force field. The QM model was mechanically embedded [31] in the MM system. The boundary between the 2 regions was treated using link hydrogen atoms. This combination of the AMBER force field and B3LYP has proven its use in many studies [32,33]. For the optimization the macro/microiterative scheme with quadratic coupling was used [34]. The calculations were done using Gaussian 09 [35].

2.2.2. Model system

Three clusters of interactions between the active site were determined by molecular dynamics simulations. Representative snapshots were chosen and optimized. First, the fully solvated structure was optimized using the AMBER99SB force field followed by aQM/MM optimization of the system with a water shell. The water shell consists of all water molecules within 0.5 nm of the system or

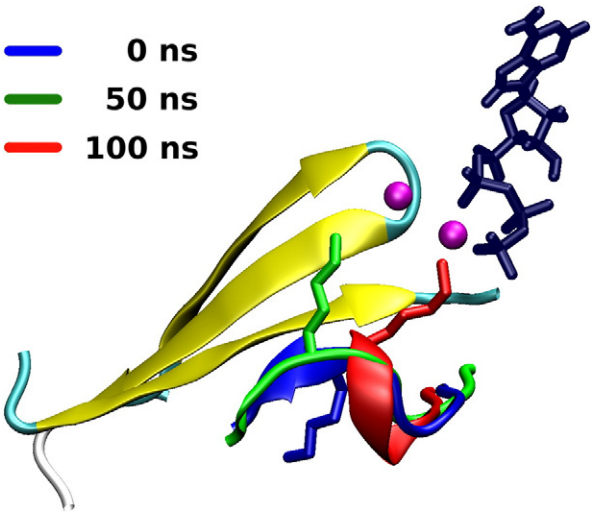

Fig. 2. Position of LYS220 at different times with respect to the active site in HIV-RT. With 0 ns the crystal structure. Adenine triphosphate (dark blue) and Mg^{2+} of the active site are shown together with the structural domain containing LYS220.

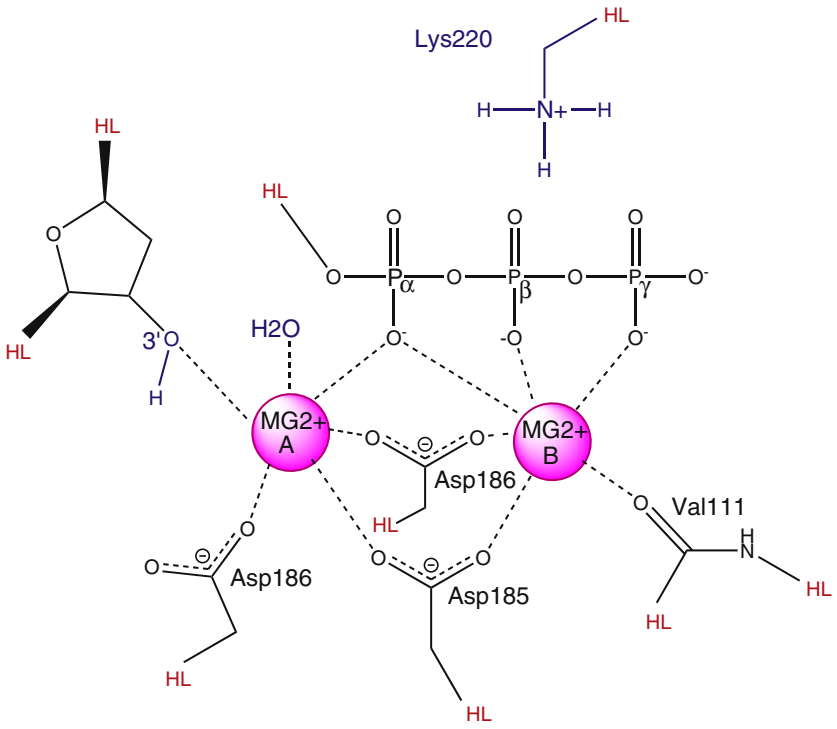

Fig. 3. The QM region used for the QM/MM optimizations. Red parts are the link atoms. Blue parts are elements of the active site that only appear after modeling (3′ hydroxyl) or molecular dynamics simulations (H2O and LYS220).

within 1.2 nm of the deoxyadenosine triphosphate substrate. Fig. 3 shows the basic QM-region applied in the present work. The triphosphate moiety of dATP was included. Both Mg^{2+} ions are coordinated by 6 ligands, indicated by the broken line, and the entire coordination shell is treated on the QM-level. The full final sugar of the primer strand was included to avoid cutting the ring system. Additionally LYS220 was added since MD simulations demonstrated the interaction with the substrate. Additional elements were added in the structure where LYS220 has water mediated hydrogen bonds with the triphosphate moiety. In this structure the water mediating the bond is included, but also ASP67, which forms a salt bridge with LYS220 in this structure.

All residues which have an atom within 0.6 nm of the QM-region were treated as being flexible during the optimization, residues further away were kept fixed. The input for Gaussian 09 was prepared using a toolkit developed by Tao and Schlegel [36] to assist ONIOM calculations.

3. Results and discussion

To understand the role of LYS220, molecular dynamics (MD) simulations were made with the AMBER 99SB force field using the GROMACS simulation package. The complex was simulated for 1 μs. The evolution of the position of LYS220 toward the triphosphate moiety is shown in Fig. 4A. Initially LYS220 stays in the crystallographic position where it is part of a beta sheet. The strand containing LYS220 has only 2 hydrogen bonds connecting it to the rest of the sheet. After 30 ns of simulation the LYS220 detaches from the beta sheet. During the next 40 ns the loop explores the conformational space, in which it rotates towards the active site with the head group directed toward the protein. A snapshot at 50 ns is shown in green in Fig. 2. After 90 ns LYS220 enters a regime in which it is tightly bounded to the triphosphate. A snapshot at 100 ns is shown in red in Fig. 2. LYS220 is now part of a 3_{10}-helix formed by LYS220 and PRO217. During the remaining 300 ns LYS220 stays within 1 nm of the triphosphate. Studying the distance, hydrogen bonds and water mediated hydrogen bonds we can discriminate between three states of interaction.

To validate the different states, representative structures of each cluster were optimized using QM/MM. The QM/MM minimized structures are shown in Fig. 5. In structure I, between 92 and 112 ns, LYS220 is within 0.37 nm of triphosphate and in tight interaction via multiple direct hydrogen bonds with Pα and Pγ. The N – H bond length of the lysine NH_3 head group forming a hydrogen bond with the terminal phosphate is elongated from about 0.105 nm to 0.118 nm, indicating that this proton is more acidic in this state. Proton transfer to the terminal phosphate could be followed by transfer to the oxygen between Pα and Pβ. This would be a substrate assisted proton transfer initiated by lysine. In structure II, between 112 ns and 150 ns, the LYS220-triphosphate distance is about 0.7 nm. Here hydrogen bond interaction between LYS220 and triphosphate is mediated by one or more water molecules (see Figs. 4 and 5). Notably this second state can also explain the experiments of Castro et al. since a water mediated proton transfer can also be catalyzed by LYS220. This has been shown for T7 DNA polymerase [37]. Structure II in Fig. 5 shows an example of a water mediated hydrogen bond. In this structure LYS220 could also catalyze water mediated proton transfer. In this state ASP67 forms a salt bridge with LYS220, which could tune the pKa of lysine. In structure III, between 150 and 180 ns, LYS220 is mostly bounded to the γ-phosphate via direct hydrogen bonds and is at a distance of 0.41 nm from LYS220. During the rest of the simulation the three states appear repeatedly.

To date, only three HIV-RT crystal structures which contain both the natural substrate and DNA are publicly available. In all three crystal structures, LYS220 is located in a beta-sheet and oriented away from the active site. To provide an extra assessment of the flexibility we studied 134 available HIV-RT crystal structures which were crystallized with different experimental conditions; namely, without

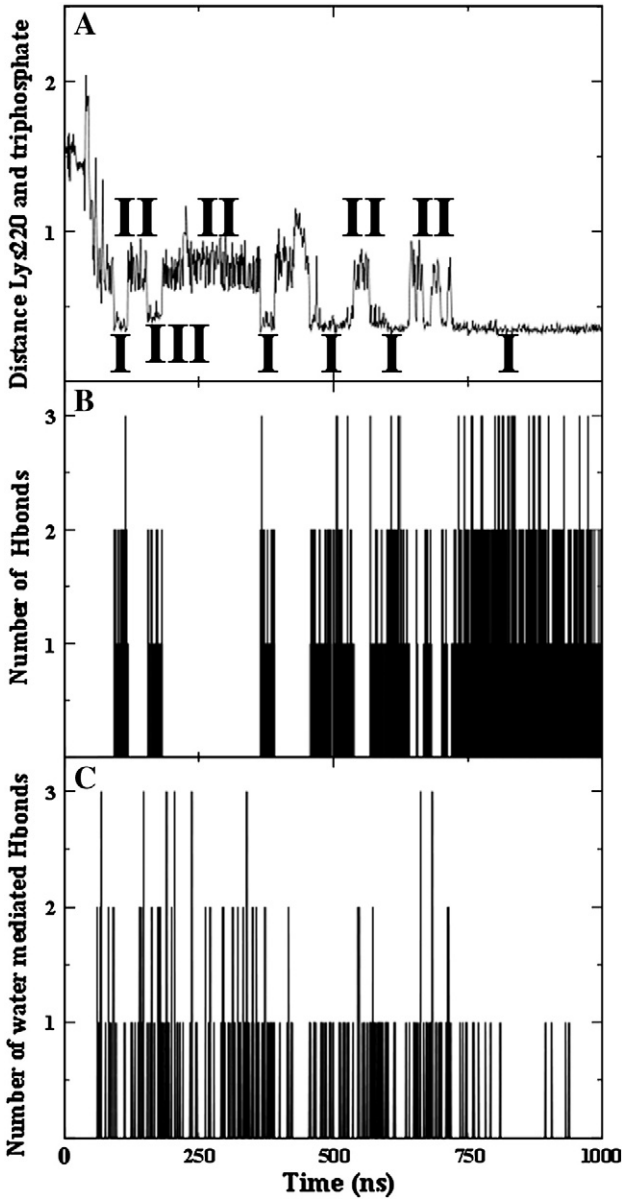

Fig. 4. Evolution in time of the interaction between LYS220 and triphosphate: (A) the center of mass distance between the NH3 head group of LYS220 and center of mass of triphosphate, labels I,II,III correspond to the structures in Fig. 5. (B) The number of direct hydrogen bonds between LYS220 and triphosphate. (C) The number of water mediated hydrogen bonds between LYS220 and triphosphate.

substrate, without nucleic acid, with non-nucleoside like drugs, and so forth. Here, the interaction between LYS220 and the substrate cannot be studied, but both the flexibility of the structural element, of which LYS220 is part, and its secondary structure can be examined. As shown in Fig. 6, the loop containing LYS220 is very flexible considering the ensemble of available crystal structures. This is on par with the results of the MD simulation and is also confirmed by hydrogen deuterium exchange rates measured by mass spectrometry [38]. Moreover in 24% of all crystal structures LYS220 is part of a 3_{10}-helix, for 7% it belongs to a beta sheet and in 69% to a loop. The flexibility observed in the ensemble of non ternary crystal structures together with the existence of the 3_{10}-helix reinforces the validity of the simulation results.

Two other lysine residues, LYS70 and LYS219, which are initially much closer to the active site, also show a very dynamic behavior. Castro et al. [7] state that LYS219 can be ruled out as proton donor by comparison with HIV-2, where LYS219 is absent but the DNA polymerase activity is similar [39]. On the same basis one can rule out LYS70. In addition, the fact that the mutation of LYS220 done by Castro et al. [7], decreases the turnover rate shows that LYS70 and LYS219 cannot fully function as alternative for LYS220.

4. Conclusions

Extensive MD simulation demonstrated the dynamics of LYS220 and revealed for the first time several states that can explain its catalytic role in nucleic acid transfer. Simulations at a higher level of theory indicated that the states found using force field methods are also valid minima on a quantum mechanical potential energy surface. This dynamic behavior of LYS220 is also observed in the ensemble of crystal structures which are crystallized without nucleic acid and substrate. Moreover, the presence of the 3_{10}-helix is also observed for some of these structures. The structural basis for the interaction between triphosphate and LYS220, proposed in this work, is of major importance for further study of the detailed mechanism for nucleotidyl transfer in HIV-RT.

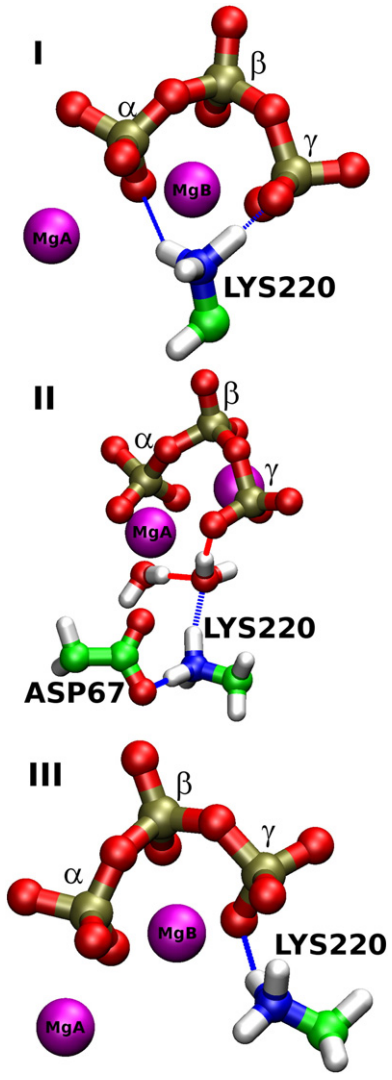

Fig. 5. The different modes of interaction between triphosphate and LYS220 after QM/MM optimization. Structure I shows the tight interaction with α and γ phosphate, II shows the state with water mediated interaction, and III the state with interaction with the terminal phosphate.

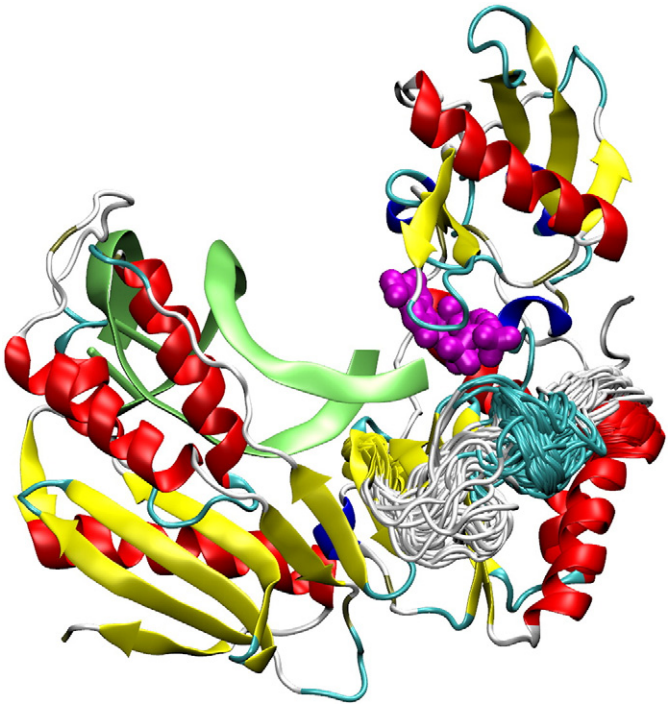

Fig. 6. The polymerase domain of HIV-RT of crystal structure 1RTD, including DNA (green) and thymidine triphosphate substrate (magenta). 134 other crystal structures were superimposed via a least squares fit onto this structure using protein backbone atoms of residues 205 to 210 and 228 to 233. The loops containing residues 210 to 228 of the 134 structures superimposed onto 1RTD are shown.

Acknowledgements

This work has been supported by the Fund for Scientific Research-Flanders (FWO). This research was conducted utilizing high-performance computational resources provided by the University of Leuven (http://ludit.kuleuven.be/hpc).

References

[1] O. Adelfinskaya, M. Terrazas, M. Froeyen, P. Marliere, K. Nauwelaerts, P. Herdewijn, Polymerase-catalyzed synthesis of DNA from phosphoramidate conjugates of deoxynucleotides and amino acids, Nucleic Acids Research 35 (2007) 5060–5072.
[2] J. Florian, M. Goodman, A. Warshel, Computer simulation of the chemical catalysis of DNA polymerases: discriminating between alternative nucleotide insertion mechanisms for T7 DNA polymerase, Journal of The American Chemical Society 125 (2003) 8163–8177.
[3] S. Michielssens, N.T. Trung, M. Froeyen, P. Herdewijn, M.T. Nguyen, A. Ceulemans, Hydrolysis of aspartic acid phosphoramidate nucleotides: a comparative quantum chemical study, Physical Chemistry Chemical Physics 11 (2009) 7274–7285.
[4] M. Fothergill, M. Goodman, J. Petruska, A. Warshel, Structure–energy analysis of the role of metal ions in phosphodiester bond hydrolysis by DNA-polymerase-I, Journal of The American Chemical Society 117 (1995) 11619–11627.
[5] T. Steitz, Structural biology — a mechanism for all polymerases, Nature 391 (1998) 231–232.
[6] C. Castro, E. Smidansky, K.R. Maksimchuk, J.J. Arnold, V.S. Korneeva, M. Gotte, W. Konigsberg, C.E. Cameron, Two proton transfers in the transition state for nucleotidyl transfer catalyzed by RNA and DNA-dependent RNA and DNA polyrnerases, Proceedings of the National Academy of Sciences of The United States of America 104 (2007) 4267–4272.
[7] C. Castro, E.D. Smidansky, J.J. Arnold, K.R. Maksimchuk, I. Moustafa, A. Uchida, M. Gotte, W. Konigsberg, C.E. Cameron, Nucleic acid polymerases use a general acid for nucleotidyl transfer, Nature Structural & Molecular Biology 16 (2009) 212–218.
[8] E.B. Lansdon, D. Samuel, L. Lagpacan, K.M. Brendza, K.L. White, M. Hung, X. Liu, C.G. Boojamra, R.L. Mackman, T. Cihlar, A.S. Ray, M.E. McGrath, S. Swaminathan, Visualizing the molecular interactions of a nucleotide analog, GS-9148, with HIV-1 reverse transcriptase-DNA complex, Journal of Molecular Biology 397 (2010) 967–978.
[9] K. Das, R.P. Bandwar, K.L. White, J.Y. Feng, S.G. Sarafianos, S. Tuske, X. Tu, J.A.D. Clark, P.L. Boyer, X. Hou, B.L. Gaffney, R.A. Jones, M.D. Miller, S.H. Hughes, E. Arnold, Structural basis for the role of the K65R mutation in HIV-1 reverse transcriptase polymerization, excision antagonism, and tenofovir resistance, Journal of Biological Chemistry 284 (2009) 35092–35100.
[10] H. Huang, R. Chopra, G. Verdine, S. Harrison, Structure of a covalently trapped catalytic complex of HIV-I reverse transcriptase: implications for drug resistance, Science 282 (1998) 1669–1675.
[11] V. Hornak, R. Abel, A. Okur, B. Strockbine, A. Roitberg, C. Simmerling, Comparison of multiple amber force fields and development of improved protein backbone parameters, Proteins: Structure, Function, and Bioinformatics 65 (2006) 712–725.
[12] A. Perez, I. Marchan, D. Svozil, J. Sponer, I.T.E. Cheatham, C.A. Laughton, M. Orozco, Refinement of the AMBER force field for nucleic acids: improving the description of alpha/gamma conformers, Biophysical Journal 92 (2007) 3817–3829.
[13] K. Meagher, L. Redman, H. Carlson, Development of polyphosphate parameters for use with the AMBER force field, Journal of Computational Chemistry 24 (2003) 1016–1025.
[14] J. Gordon, J. Myers, T. Folta, V. Shoja, L. Heath, A. Onufriev, H++: a server for estimating pK(a)s and adding missing hydrogens to macromolecules, Nucleic Acids Research 33 (2005) W368–W371.
[15] M.H.M. Olsson, C.R. Sondergaard, M. Rostkowski, J.H. Jensen, PROPKA3: consistent treatment of internal and surface residues in empirical pK(a) predictions, Journal of Chemical Theory and Computation 7 (2011) 525–537.
[16] D. A. Case, T. E. Cheatham III, C. L. Simmerling, J. Wang, R. E. Duke, R. Luo, M. Crowley, R. C. Walker, W. Zhang, K. M. Merz, B. Wang, S. Hayik, A. Roitberg, G. Seabra, I. Kolossvary, K. F. Wong, J. Paesani, J. Vanicek, X. Wu, S. Brozell, T. Steinbrecher, H. Gohlke, L. Yang, C. Tan, J. Morgan, V. Hornak, G. Cui, D. H. Mathews, M. G. Seetin, C. Sagui, V. Babin, P. A. Kollman, Amber 10, 2008.
[17] A.J. DePaul, E.J. Thompson, S.S. Patel, K. Haldeman, E.J. Sorin, Equilibrium conformational dynamics in an RNA tetraloop from massively parallel molecular dynamics, Nucleic Acids Research 38 (2010) 4856–4867.
[18] E. Sorin, V. Pande, Exploring the helix-coil transition via all-atom equilibrium ensemble simulations, Biophysical Journal 88 (2005) 2472–2493.
[19] M. Mahoney, W. Jorgensen, A five-site model for liquid water and the reproduction of the density anomaly by rigid, nonpolarizable potential functions, Journal of Chemical Physics 112 (2000) 8910–8922.
[20] B. Hess, C. Kutzner, D. van der Spoel, E. Lindahl, GROMACS 4: algorithms for highly efficient, load-balanced, and scalable molecular simulation, Journal of Chemical Theory and Computation 4 (2008) 435–447.
[21] U. Essmann, L. Perera, M. Berkowitz, T. Darden, H. Lee, L. Pedersen, A smoot particle mesh ewald method, Journal of Chemical Physics 103 (1995) 8577–8593.
[22] B. Hess, P-LINCS: a parallel linear constraint solver for molecular simulation, Journal of Chemical Theory and Computation 4 (2008) 116–122.
[23] G. Bussi, T. Zykova-Timan, M. Parrinello, Isothermal-isobaric molecular dynamics using stochastic velocity rescaling, Journal of Chemical Physics 130 (2009) 074101 9 pp.
[24] M. Parrinello, A. Rahman, Polymerphic transitions in single-crystals — a new molecular-dynamics method, Journal of Applied Physics 52 (1981) 7182–7190.
[25] S. Dapprich, I. Komaromi, K. Byun, K. Morokuma, M. Frisch, A new ONIOM implementation in Gaussian98. Part I. The calculation of energies, gradients, vibrational frequencies and electric field derivatives, Journal of Molecular Structure: Theochem 461 (1999) 1–21.
[26] T. Vreven, K. Morokuma, Investigation of the S-0 to S-1 excitation in bacteriorhodopsin with the ONIOM(MO : MM) hybrid method, Theoretical Chemistry Accounts 109 (2003) 125–132.
[27] M. Svensson, S. Humbel, R. Froese, T. Matsubara, S. Sieber, K. Morokuma, ONIOM: A multilayered integrated MO + MM method for ge-ometry optimizations and single point energy predictions. A test for Diels–Alder reactions and Pt(P(t-Bu)(3))(2) + H-2 oxidative addition, Journal of Physical Chemistry 100 (1996) 19357–19363.
[28] A.D. Becke, Density-functional thermochemistry 3. The role of exact exchange, Journal of Chemical Physics 98 (1993) 5648–5652.
[29] N. Godbout, D.R. Salahub, J. Andzelm, E. Wimmer, Optimization of gaussian-type basis-sets for local spin-density functional calculations .1. Boron through neon, optimization technique and validation, Canadian Journal of Chemistry 70 (1992) 560–571.
[30] C. Sosa, J. Andzelm, B.C. Elkin, E. Wimmer, K.D. Dobbs, D.A. Dixon, A local density functional-study of the structure and vibrational frequencies of molecular transition-metal compounds, Journal of Physical Chemistry 96 (1992) 6630–6636.
[31] F.R. Clemente, T. Vreven, M.J. Firsch, Chapter 2. Getting the most out of oniom: guidelines and pitfalls, Quantum Biochemistry (2010) 63.
[32] M. Torrent, T. Vreven, D. Musaev, K. Morokuma, O. Farkas, H. Schlegel, Effects of the protein environment on the structure and energetics of active sites of metalloenzymes. ONIOM study of methane monooxygenase and ribonucleotide reductase, Journal of the American Chemical Society 124 (2002) 192–193.
[33] T. Vreven, K. Morokuma, On the application of the IMOMO (integrated molecular orbital plus molecular orbital) method, Journal of Computational Chemistry 21 (2000) 1419–1432.
[34] T. Vreven, M. Frisch, K. Kudin, H. Schlegel, K. Morokuma, Geometry optimization with QM/MM methods II: explicit quadratic coupling, Molecular Physics 104 (2006) 701–714.
[35] M.J. Frisch, G.W. Trucks, H.B. Schlegel, G.E. Scuseria, M.A. Robb, J.R. Cheeseman, J.J.A. Montgomery, T. Vreven, K.N. Kudin, J.C. Burant, J.M. Millam, S.S. Iyengar, J. Tomasi, V. Barone, B. Mennucci, M. Cossi, G. Scalmani, N. Rega, G.A. Petersson, H. Nakatsuji, M. Hada, M. Ehara, K. Toyota, R. Fukuda, J. Hasegawa, M. Ishida, T. Nakajima, Y. Honda, O. Kitao, H. Nakai, M. Klene, X. Li, J.E. Knox, H.P. Hratchian,

J.B. Cross, V. Bakken, C. Adamo, J. Jaramillo, R. Gomperts, R.E. Stratmann, O. Yazyev, A.J. Austin, R. Cammi, C. Pomelli, J.W. Ochterski, P.Y. Ayala, K. Morokuma, G.A. Voth, P. Salvador, J.J. Dannenberg, V.G. Zakrzewski, S. Dapprich, A.D. Daniels, M.C. Strain, O. Farkas, D.K. Malick, A.D. Rabuck, K. Raghavachari, J.B. Foresman, J.V. Ortiz, Q. Cui, A.G. Baboul, S. Clifford, J. Cioslowski, B.B. Stefanov, G. Liu, A. Liashenko, P. Piskorz, I. Komaromi, R.L. Martin, D.J. Fox, T. Keith, M.A. Al-Laham, C.Y. Peng, A. Nanayakkara, M. Challacombe, P.M.W. Gill, B. Johnson, W. Chen, M.W. Wong, C. Gonzalez, J.A. Pople, RevisionA.1, Gaussian 09, Gaussian, Inc, Wallingford, CT, 2009.

[36] P. Tao, H.B. Schlegel, Software news and updates a toolkit to assist ONIOM calculations, Journal of Computational Chemistry 31 (2010) 2363–2369.

[37] L. Wang, S. Broyde, Y. Zhang, Polymerase-tailored variations in the water-mediated and substrate-assisted mechanism for nucleotidyl transfer: insights from a study of T7 DNA polymerase, Journal of Molecular Biology 389 (2009) 787–796.

[38] J. Seckler, K. Howard, M. Barkley, P. Wintrode, Solution structural dynamics of HIV-1 reverse transcriptase heterodimer, Biochemistry 48 (2009) 7646.

[39] A. Hizi, R. Tal, M. Shaharabany, S. Loya, Catalytic properties of the reverse transcriptases of human immunodeficiency viruses type-1 and type-2, Journal of Biological Chemistry 266 (1991) 6230–6239.